

## Highlights

### Flow-Induced Buckling of a Viscoelastic Bistable Structure in Time Varying Flow

Leixin Ma, Varshitha Janavi, Uday Kumar Punna

- The interaction between fluid flows and viscoelastic bistable structures is analyzed under time-varying flow conditions.
- The role of viscoelasticity in modulating structural strain energy during snap-through transitions is elucidated.
- A predictive framework based on a modified Cauchy number is developed to quantify the coupling between viscoelastic material properties and fluid loading.
- The viscoelastic structure can adapt its stiffness to different flow acceleration rates.

# Flow-Induced Buckling of a Viscoelastic Bistable Structure in Time Varying Flow

Leixin Ma<sup>a</sup>, Varshitha Janavi<sup>a</sup>, Uday Kumar Punna<sup>a</sup>

<sup>a</sup>School for Engineering of Matter, Transport & Energy, Arizona State University, AZ 85287, USA,

---

## Abstract

This study investigates the influence of linear viscoelasticity on the snap-through dynamics of bistable structures subjected to fluid flows with changing speed. The viscoelastic behavior is modeled using a Prony series, capturing the time-dependent relaxation modulus. Numerical simulations based on the Arbitrary Lagrangian-Eulerian framework are conducted to analyze the structural response under changing flow speeds. Key parameters, including relaxation times and Prony coefficients, are systematically evaluated to elucidate their roles in governing dynamic stability and energy transfer between the fluid and structure systems. Two critical dimensionless parameters are identified: a Cauchy number modified by viscoelastic stiffness and the Deborah number. The modified Cauchy number quantifies the interaction between fluid forces and effective structural stiffness, while the Deborah number captures the transition between viscous-dominated and elastic-dominated regimes. Structures with significant viscous effects exhibit delayed buckling and increased strain energy under faster inlet flow acceleration, indicating a stiffness amplification effect. These findings provide insight into the interplay between viscoelastic material response and flow conditions and inform the design of adaptive bistable structures for applications in soft robotics, morphing surfaces, and energy-harvesting technologies.

*Keywords:* Viscoelasticity; Bistability; Fluid-structure interaction; Flexible structures

---

## 1. Introduction

Bistable structures, characterized by their ability to switch between two stable equilibrium states, have gained significant attention for their potential applications in soft robotics, morphing surfaces, and energy harvesting [1]. These structures undergo significant deformation during snap-through transitions, enabling rapid actuation, locomotion, and energy dissipation [2, 3, 4].

Traditional studies predominantly address bistable structures made of linear elastic materials, where the material property is time independent of external loads [2]. However, in practical applications, materials such as silicone elastomers—commonly used in soft robotics—often exhibit viscoelastic behavior, combining time-dependent viscous and elastic responses [5]. Such behavior significantly influences energy storage, dissipation, and dynamic stability during snap-through transitions [6]. Understanding the role of time-dependent material properties is essential to optimize these structures for applications requiring adaptive performance under dynamic conditions.

Moreover, the Fluid-Structure Interaction (FSI) amplifies the complexity of snap-through dynamics[7, 8, 9, 10]. Fluid forces interact with the structure, inducing snap-through buckling and influencing vortex shedding and hydrodynamic force distribution. While previous research has examined fluid-structure interaction (FSI) effects on flexible structures in fluid flows, the interplay between the viscoelasticity structure dynamics and fluid flows remains poorly understood. This coupling is especially critical in applications such as underwater technologies and morphing structures, where optimizing performance requires careful control of both material properties and flow conditions[11, 12, 13].

Understanding the dynamics of viscoelastic materials has long been of interest to mechanicians. Chen et al. [14] demonstrated that the bistable behavior of viscoelastic shells can be spatiotemporally programmed through tailored shell geometry and material properties, enabling precise control over snap-through transitions. Gomez et al. [15] further investigated viscoelastic snap-through under mechanical loading, showing that time-dependent material relaxation significantly influences transition timing and energy dissipation. While progress has been made in modeling viscoelastic behavior [16], the combined effects of viscoelastic relaxation and fluid-induced forces on bistable transitions remain insufficiently explored.

This work addresses these gaps by investigating the snap-through dynamics of viscoelastic bistable beams under time-varying flows, where the flow speed slowly ramps up from zero to maximum. The viscoelastic behavior is modeled using a Prony series to represent the relaxation modulus, allowing systematic exploration of the effects of relaxation times and Prony coefficients on structural response and stiffness modulation. Numerical simulations based on the Arbitrary Lagrangian-Eulerian (ALE) method capture the coupled dynamics between fluid loading and flow-induced deformation. Through these simulations, the study identifies and analyzes two key dimensionless parameters governing snap-through behavior: the Deborah number and a viscoelastic-modified Cauchy number, which together characterize the interplay between material relaxation and fluid-structure interaction.

One distinctive feature of viscoelastic materials is their time-dependent response, which leads to changes in the system's energy—effectively mimicking adaptive stiffness. In fluid-structure systems, varying structural stiffness is crucial for controlling mechanical performance. For instance, fish maintain high swimming efficiency across a wide range of speeds by actively tuning tail flexibility through muscle activation, effectively modulating stiffness [17]. When fluid flows around flexible structures, stiffness plays a key role in governing flow-induced vibrations and the energy transfer between the fluid and the structure [12, 18, 19]. Compared to active stiffness tuning methods that rely on external control mechanisms—such as jamming-based systems [20]—viscoelasticity offers a passive and materially intrinsic alternative. By responding to strain rate, temperature, or frequency, viscoelastic materials enable automatic stiffness modulation without the need for external actuation.

By integrating viscoelastic modeling with fluid-structure interaction analysis, this research extends previous work by highlighting the mechanisms governing snap-through behavior. The insights gained from this study contribute to advancing design strategies for applications that require adaptive energy storage, such as morphing surfaces, soft robotics, and energy-harvesting devices [21, 16].

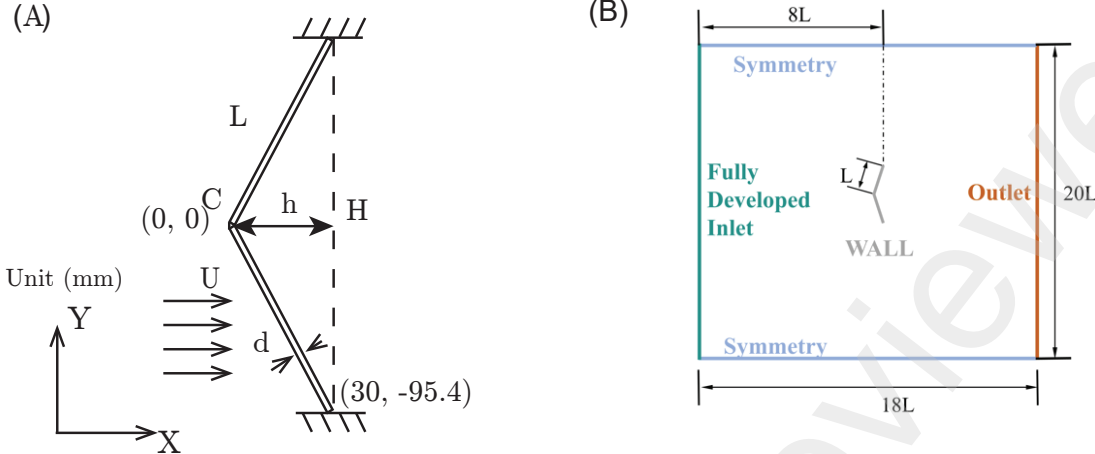


Figure 1: A sketch of the fluid structure interaction analysis of (A) a bistable beam with two ends fixed. (B) The simulation set up.

## 2. Description of model setup

The initial stress-free state of bistable flexible structure is depicted in Figure 1 (A). This design can be thought of as a 2D simplification of recently developed deployable bistable structures by [22] and [2]. The system consists of two sections with a length of  $L$  and a thickness of  $d$  connected at the rigid center point, designated as point C. The geometry is modeled as a continuous beam, so there is no need to model a joint specifically. The other edge of each beam section is fixed along the center axis, which is represented by the dashed line. The initial distance between the center point and the dashed center line is defined as the initial height of the system, which is denoted as  $h$ . Meanwhile, since the total length of the beams is larger than the distance between the two fixed edges  $H$ , the beams cannot be stress-free when the center point passes through the center axis. From our previous quasi-static, displacement-controlled loading at the center point C—mimicking a three-point bending test using a universal testing machine in structural mechanics experiments—we found that the system exhibits two stable states with minimum strain energy. As long as the external energy exceeds the energy difference between the local maximum strain energy and the initial strain energy, the structure can quickly switch to the other stable state without needing external energy input. This phenomenon is known as snap-through buckling.

To investigate the fluid-structure interaction (FSI) for viscoelastic bistable structures, we analyze the passive deformation of a viscoelastic beam subjected to gradually increasing fluid flows. The time-varying inlet flow velocity, denoted as  $U(t)$ , follows a ramp profile, where we systematically adjust the flow acceleration rate  $q$  from  $q = 0.005$  to  $q = 0.02$  m/s. The fluid viscosity is set to  $\mu_{\text{fluid}} = 0.2$  Ns/m<sup>2</sup>, and the fluid density is set to  $\rho_{\text{fluid}} = 1000$  kg/m<sup>3</sup>. In this study, the characteristic length is defined as the vertical distance between the fixed ends of the beam, with the Reynolds number ranging from 0 to 150.

The viscoelastic behavior of the beam is modeled using the Prony series. The relaxation modulus  $G(t)$  are adjusted by changing the relaxation time  $\tau$  and Prony coefficient  $g$ . Table 1 shows the range of structural and flow features modeled in this paper. Parametric studies are conducted to systematically explore the effects of varying the relaxation modulus. These

Symbol	Value	Unit	Description
$L$	100	mm	Beam length
$d$	2	mm	Beam thickness
$h$	30	mm	Beam initial height
$E_0$	$8.9 \times 10^5$	Pa	Instantaneous Young's modulus
$\tau$	1 – 100	s	Relaxation time
$g$	0.2 – 0.8		Prony coefficient
$\nu$	0.49	1	Poisson's ratio
$\rho$	3500	kg/m <sup>3</sup>	Structure density
$\mu_{\text{fluid}}$	0.2	Ns/m <sup>2</sup>	Fluid dynamic viscosity
$\rho_{\text{fluid}}$	1000	kg/m <sup>3</sup>	Fluid density
$U$	0 - 0.15	m/s	Flow speed

Table 1: Parameters with symbolic representations for reference case.

simulations are designed to understand fluid-induced buckling in soft viscoelastic materials. By studying this fundamental problem, we aim to introduce viscoelastic properties into the bistable systems proposed in [22, 2], thereby enabling the design of structures with tunable dynamic behavior in fluid environments.

### 3. Computational fluid-structure interaction analysis

#### 3.1. Governing equations

The governing equations of the laminar viscous fluid flow in the present numerical analysis, namely the Navier-Stokes equations, are expressed as follows.

$$\frac{\partial \rho_f}{\partial t} + \nabla \cdot (\rho_f \mathbf{U}_f) = 0 \quad (1)$$

$$\rho_f \frac{\partial \mathbf{U}_f}{\partial t} + \rho_f (\mathbf{U}_f \cdot \nabla) \mathbf{U}_f = \nabla \cdot [-p \mathbf{I} + \boldsymbol{\tau}] + \mathbf{F} \quad (2)$$

where  $\rho_f$ ,  $\mathbf{U}_f$ ,  $p$ ,  $\boldsymbol{\tau}$ ,  $\mathbf{F}$  stand for the fluid density, the fluid velocity vector, the pressure, the viscous stress tensor, and the volume force vector, respectively.  $\mathbf{I}$  is an identity tensor. The viscous stress tensor,  $\boldsymbol{\tau}$ , can be calculated as follows.

$$\boldsymbol{\tau} = 2\mu \mathbf{S} - \frac{2}{3}\mu(\nabla \cdot \mathbf{U}_f)\mathbf{I} \quad (3)$$

where  $\mu$  denotes the dynamic viscosity of a fluid.  $\mathbf{S}$  is the strain-rate tensor:

$$\mathbf{S} = \frac{1}{2} [\nabla \mathbf{U}_f + (\nabla \mathbf{U}_f)^T] \quad (4)$$

For structural dynamics, the deformation of solid structures is governed by:

$$\rho_s \frac{\partial^2 \chi_s}{\partial t^2} = \nabla \cdot \boldsymbol{\sigma}_s + F_v \quad (5)$$

where  $\rho_s$ ,  $\chi_s$ ,  $\sigma_s$  and  $F_v$  represent the density of the structure, the structural displacement, the Cauchy stress on the structure and the volumetric force, respectively. Since a linear viscoelastic material model is employed, the Cauchy stress tensor at a given time is obtained by integrating the product of the strain rate and the relaxation modulus over the history of past time instances. The constitutive relations are described in more detail in Section 4.

The finite element method (FEM) is employed to discretize the aforementioned Navier-Stokes equations and the linear elastic solid structure's governing equations. The quantities are stored at the nodes of the elements when constructing the fields. In the present study, a segregated approach is adopted to solve the governing equations sequentially, which allows for the decoupling of the pressure and velocity, rather than employing a monolithic approach. For the spatial discretization, second-order polynomials are used for fluid velocity  $\mathbf{U}_f$ , and first order polynomials are used for pressure  $p$ .

In addition, second-order polynomials are employed for displacement  $\partial^2\chi_s$ . Quadrature Gaussian integration scheme is used to handle the divergence, gradient, and Laplacian terms of the Navier-Stokes equations. The second-order backward difference method is applied for the discretization of the time iteration. The Laplacian term in the structure's governing equation adopts the second-order integration scheme. After the global matrix is assembled, the PARDISO solver is used to solve the global matrix of the large sparse linear systems.

### *3.2. Arbitrary Lagrangian-Eulerian method*

The Arbitrary Lagrangian-Eulerian (ALE) method is applied to solve this fluid-structure interaction problem based on the finite element mesh in COMSOL v6.0 [23]. The ALE scheme formulates the fluid domain equations using the Eulerian description in a spatial frame, while the equations of the structural deformation are formulated based on the Lagrangian description in a material frame. The spatial frame means that the coordinate axes are fixed in a spatial coordinate system. In a material frame, the coordinate axes are fixed to the material in the reference configuration and follow the deformed solid structure. During the solid structural deformation, the spatial frame stays unchanged, while the material coordinate system has undergone deformation in accordance with the structural deformation. Meanwhile, the material coordinates of each material point remain constant, however, its spatial coordinates have been altered. More details of the FSI coupling in ALE method are described in [7].

Smoothing methods such as Laplace smoothing, Winslow smoothing, and Yeoh smoothing can be applied to move the mesh of the flow domain. The Yeoh smoothing model [24, 25, 26] is employed here, which is inspired by hyperelastic materials. Yeoh smoothing generally produces the best results and allows the largest displacement of boundaries before mesh elements become inverted. The laminar flow is solved by direct numerical simulation (DNS). To solve for pressure and velocity, the incremental pressure-correction method is employed for the Navier-Stokes equations. The algorithm proceeds as follows: first, each velocity component is solved sequentially; next, the Poisson equation is solved to correct the pressure; and finally, the velocity components are updated with the corrected values.

### *3.3. Fluid-structure coupling*

The two-way fluid-structure coupling method used in the present simulations is implemented through the coupling at the interface between the fluid and solid domains. The

boundary conditions at the fluid-structure interface are written as:

$$\begin{cases} \sigma_s \cdot n = \sigma_f \cdot n \\ \mathbf{u}_s = \mathbf{u}_f \end{cases} \quad (6)$$

where the subscripts  $s$  and  $f$  denote the structure and the fluid.  $\sigma_s$  and  $\sigma_f$  are the flow stress of the structure and fluid, respectively.  $\mathbf{u}_s$  and  $\mathbf{u}_f$  are the velocity of the boundary node for solid and fluid, respectively.  $n$  is the normal vector at the interface between the fluid and the solid. The strong coupling ALE method used here allows the fluid and structure field to transfer information iteratively per time step at the interface.

### 3.4. Initial conditions

The computational setup and boundary conditions are illustrated in Figure 1 (B). A fully developed inlet profile is prescribed and the fluid-structure interface is modeled as a no-slip wall. The time step size is set to 0.005 seconds to ensure sufficient temporal resolution. The corresponding Courant-Friedrichs-Lowy number (CFL) is 0.8, computed as the ratio of the product of the fluid velocity  $U$  and the time step size  $\Delta t$  to the grid spacing  $\Delta h_g$  i.e.  $CFL = \frac{U\Delta t}{\Delta h_g}$ . The  $CFL < 1$  is chosen for the robustness of the simulation [27]. The structural material is modeled as linear viscoelastic while accounting for geometric nonlinearity, with both ends fixed, as illustrated in Figure 1(A). The flow speed is defined as a normal inflow velocity, increasing from 0 m/s to 0.15 m/s linearly over time with different rates of increase. This approach enables the analysis of snap-through buckling behavior under different flow acceleration rates.

## 4. Viscoelastic material model

In viscoelastic fluid-structure interactions, the structural response is governed by the material's time-dependent relaxation modulus,  $G(t)$ , which is often described using the Prony series as:

$$G(t) = G_0 \left( 1 - \sum_{i=1}^n g_i \left( 1 - e^{-\frac{t}{\tau_i}} \right) \right), \quad (7)$$

where  $G_0$  is the instantaneous shear modulus,  $g_i$  are the Prony coefficients, and  $\tau_i$  are the relaxation times. The subscript  $i$  denotes the  $i^{\text{th}}$  branch of the Prony series.

Physically,  $G_0$  represents the material's maximum stiffness immediately after loading, corresponding to its purely elastic response at  $t = 0$ . The coefficients  $g_i$  quantify the fractional stiffness contributions of individual viscoelastic mechanisms, while  $\tau_i$  define their characteristic relaxation timescales. An equivalent representation starts with the relaxed modulus  $G_\infty$ , corresponding to the material's stiffness as  $t \rightarrow \infty$  can be written as:

$$G(t) = G_\infty + G_0 \sum_{i=1}^n g_i e^{-\frac{t}{\tau_i}},$$

where  $G_0 = G_\infty + G_0 \sum_{i=1}^n g_i$ . The relaxation times  $\tau_i$  are related to the material's viscosity  $\eta_i$  and modulus  $E_i$  for the  $i^{\text{th}}$  branch via:

$$\tau_i = \frac{\eta_i}{E_i}. \quad (8)$$

In this paper, one-branch Prony series is used. Then, the effective relaxation modulus becomes:

$$G(t) = G_0 \left( 1 - g \left( 1 - e^{-\frac{t}{\tau}} \right) \right), \quad (9)$$

where  $0 < g < 1$ .

The corresponding Young's modulus for viscoelastic material is,

$$E(t) = 2G(t)(1 + \nu) = 2G_0 \left( 1 - g \left( 1 - e^{-\frac{t}{\tau}} \right) \right) (1 + \nu) \quad (10)$$

The Deborah number (De) is a dimensionless parameter commonly used in the study of viscoelastic materials to quantify the relative importance of material relaxation time compared to the characteristic time scale of an applied deformation or observation [28, 29]:

$$\text{De} = \frac{\tau}{t_{\text{obs}}}, \quad (11)$$

where  $\tau$  represents the characteristic relaxation time, and  $t_{\text{obs}}$  is the duration over which the material's response is observed. When  $\text{De} \gg 1$ , the material behaves more elastically,  $G(t) \approx G_0$ ; when  $\text{De} \ll 1$ , the material shows a more viscous response, the material behaves softer with  $G(t) \approx G_0(1 - g)$ .

The relaxation modulus can be used to derive the creep compliance,  $J(t)$ , which characterizes the time-dependent strain response under constant stress using the Prony Series:

$$J(t) = J_0 \left( 1 + j \left( 1 - e^{-\frac{t}{\tau}} \right) \right) \quad (12)$$

where  $J_0 = 1/G_0$ , and it is the instantaneous creep modulus, defined as the reciprocal of the instantaneous elastic modulus.  $jJ_0 = J_\infty - J_0$ , and  $J_\infty = 1/G_\infty = 1/(G_0(1 - g))$

In general, when the stress is changing over time, the strain response is given by the convolution integral:

$$\varepsilon(t) = \int_0^t J(t - \tau) \frac{d\sigma(\tau)}{d\tau} d\tau \quad (13)$$

Under constant stress  $\sigma_0$ , the strain  $\varepsilon(t)$  is proportional to the creep compliance via:

$$\varepsilon(t) = \frac{\sigma_0 \cdot J(t)}{2} = \frac{\sigma_0}{2G_0(1 - g)} [1 + g (1 - e^{-t/\tau})] \quad (14)$$

Hence, the strain energy is

$$E_{\text{strain}}(t) = \frac{1}{2} \sigma_0 \varepsilon(t) = \frac{\sigma_0^2}{4G_0(1 - g)} (1 + g (1 - e^{-t/\tau})) \quad (15)$$

## 5. Verification Analysis

The accuracy and robustness of the present numerical method for fluid-structure interaction (FSI) were first validated against a well-established benchmark problem: flow past a 2D circular cylinder with an elastic splitter plate [30]. Detailed results of the verification are presented in [7]. For the bistable structure analyzed in this study, unstructured triangular meshes are employed for both the fluid and solid domains. The fluid mesh resolution

is calibrated using COMSOL Multiphysics [23], while the solid-domain mesh is constructed with mesh control entities and refined through four smoothing iterations to ensure a gradual transition in element size across the interface. A mesh sensitivity analysis was performed by analyzing the results for key solution variables across different levels of mesh refinement, as detailed in [7].

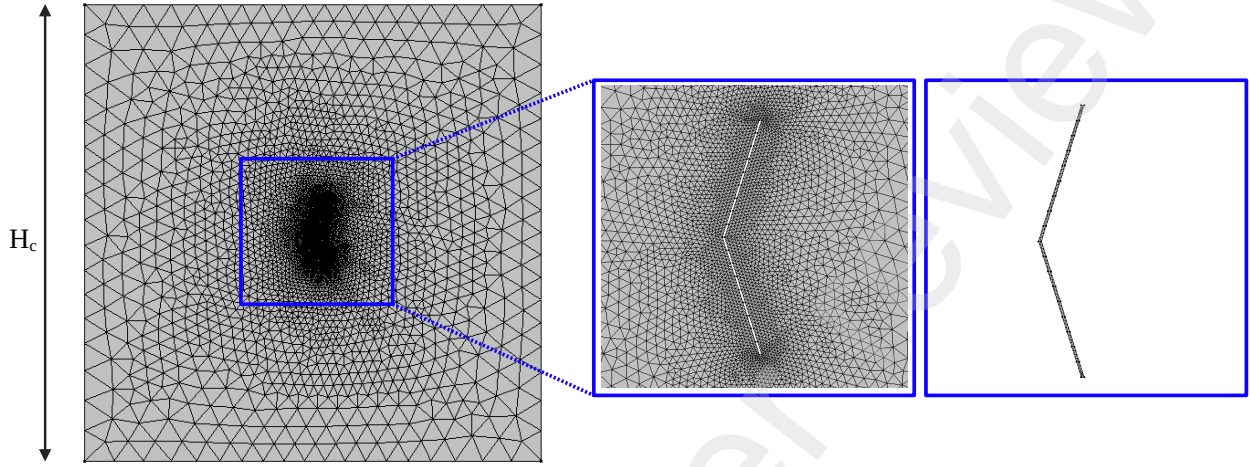


Figure 2: Unstructured triangular mesh configuration. Zoom on the fluid domain mesh around the flexible rod, and reference configuration for the solid domain mesh, respectively.

The selected mesh (Figure 2) has a maximum element size given by  $H_c/15$ , average element skewness of 0.87, and 10437 triangular elements.

Meanwhile, the viscoelastic material model was validated by comparing theoretical predictions with numerical simulations of tensile tests performed on a dogbone structure, as presented in Appendix A. The results show good agreement between the theoretical and simulated responses.

## 6. Results and discussions

### 6.1. Snap-through buckling of a linear elastic bistable beam induced by fluid

First, we investigate the flow-induced deformation of a linear elastic bistable beam characterized by a thickness-to-length ratio  $h/L = 0.3$ , elastic modulus  $E = 8.9 \times 10^5 \text{ N/m}^2$ , and Poisson's ratio  $\nu = 0.49$ . Additional fluid flow parameters are listed in Table 1. The inlet flow speed is gradually increased from 0 m/s to 0.15 m/s, with the inlet flow acceleration rate at 0.005 m/s<sup>2</sup> and 0.02 m/s<sup>2</sup>. As the flow speed increases, the structure moves to the rightward positive X direction, as illustrated in Figure 3(A-B). The fluid flow continues to transfer energy to the structure and increases its total strain energy, as shown in Figure 3(C). A critical velocity is observed at which the total strain energy reaches a local maximum, marked by the red circles in Figure 3, indicating the onset of snap-through behavior.

Beyond this critical point, further increases in flow speed cause the structure to continue deflecting in the positive x-direction, progressing toward a local strain energy minimum where the center point reaches 47 mm. This deflection continues until the displacement approaches approximately 55 mm, as shown in Figure 3(B).

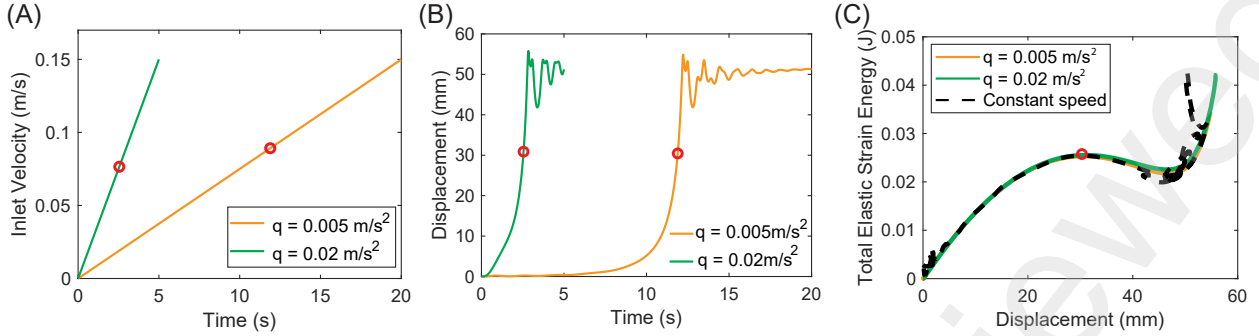


Figure 3: (A) Temporal evolution of the flow speed (B) Temporal evolution of the displacement at the center point. (C) Variation of total elastic strain energy with the displacement at the center point. The dashed line corresponds to the result in steady, uniform inlet flow with speed of  $U = 0.1 \text{ m/s}$ , and the Cauchy number is around 1.16

The dynamic process from the red point to displacement at 55 mm completes within a very short timescale. When inlet flow acceleration rate  $q = 0.02 \text{ m/s}^2$ , the dynamic process spans from 2.55 s and 2.88 s, corresponding to a flow speed increase from 0.077 m/s to 0.086 m/s. In comparison, for  $q = 0.005 \text{ m/s}^2$ , the event spans from 11.89 s to 12.2 s, with a corresponding flow speed increasing from 0.089 m/s to 0.09 m/s. This rapid transition, which is completed in approximately 0.3 s, is attributed to snap-through buckling, during which the structural strain energy sharply decreases from a local maximum (highlighted by the red circles in Figure 3) to a local minimum.

Recent findings indicate that the Cauchy number is a key dimensionless parameter governing flow-induced snap-through buckling. Following the definition in [31], the Cauchy number is defined as  $\text{Ca} = \frac{\rho U^2}{4E} \frac{L}{h} \left( \frac{L}{d} \right)^3$ , where  $\rho$  is the fluid density,  $U$  is the inlet flow velocity, and  $E$ ,  $L$ ,  $h$ , and  $d$  are the structural properties. In previous studies with steady, uniform inlet flows [7], the Cauchy number was readily defined. In the present work, where the inlet flow speed varies over time, we estimate the Cauchy number during the 0.3 s snap-through event. For  $q = 0.02 \text{ m/s}^2$ , the critical Cauchy number ranges from approximately 0.70 to 0.86; for  $q = 0.005 \text{ m/s}^2$ , it ranges from 0.92 to 0.94. These values are consistent with the critical Cauchy number of approximately 0.9, previously identified as the threshold for initiating buckling under constant uniform flows.

One notable observation is that the structure tends to undergo snap-through buckling at slightly lower flow speeds or Cauchy numbers when subjected to a higher inlet flow acceleration. This difference suggests that flow inertia may have an influence on the fluid-structure interaction process [32]. Despite variations in the critical Cauchy number, the overall evolution of the total elastic strain energy remains nearly identical, with only minor discrepancies observed at the local energy minimum. Additionally, we compare the strain energy variation with a representative case under a steady, uniform inlet flow at  $U = 0.1 \text{ m/s}$  (corresponding to  $\text{Ca} = 1.16$ ), which lies near the critical threshold for snap-through buckling reported in [7]. The resulting strain energy profile closely resembles those observed under time-varying inlet flow conditions. This comparison indicates that, for a linear elastic material, the total strain energy change associated with snap-through buckling is largely insensitive to the rate at which the flow speed increases.

Following the snap-through buckling event, the structure undergoes oscillations around the configuration corresponding to the local energy minimum, despite the continued increase in flow speed. These oscillations gradually decay as the system dissipates the energy in fluid.

### 6.2. Snap-through buckling of a viscoelastic bistable beam induced by fluid

We perform a coupled fluid-structure interaction analysis of a viscoelastic beam with the same geometry as the linear elastic structure. The inlet flow velocity  $U(t)$  increases linearly from 0 to 0.15 m/s over time. The inlet flow acceleration rate is varied across three cases: 0.005 m/s<sup>2</sup>, 0.01 m/s<sup>2</sup>, and 0.02 m/s<sup>2</sup>.

The viscoelastic material is modeled using a one-branch Prony series, with an instantaneous modulus of  $2.99 \times 10^5$  Pa. The Prony coefficient  $g$  ranges from 0.2 to 0.7, and the relaxation time  $\tau$  is varied over 1, 5, 10, and 100 seconds.

Figure 4 presents the variation of the critical flow speed corresponding to the maximum structural strain energy as a function of the Prony coefficient  $g$ . Subfigures (A)–(C) correspond to inlet flow accelerations at 0.005 m/s<sup>2</sup>, 0.01 m/s<sup>2</sup>, and 0.02 m/s<sup>2</sup>, respectively. Similar to the linear elastic case, an increase in the inlet flow acceleration results in a decrease in the critical flow speed required to trigger snap-through buckling.

As the  $\tau$  increases at a constant inlet flow acceleration and constant  $g$ , the buckling phenomenon does not occur until the flow speed reaches a higher critical value. According to Equation 9, the material is more elastic and stiffer at higher  $\tau$ , therefore necessitating greater flow-induced energy to initiate buckling.

As the  $g$  increases and  $\tau$  is held constant, the material exhibits more pronounced viscoelastic behavior, characterized by increased time-dependent deformation under load. This enhanced viscoelasticity can lead to delayed buckling phenomena, where the structure remains stable for a finite duration before suddenly collapsing. This phenomenon is analogous to the delayed buckling of viscoelastic spherical shells under constant subcritical pressure, as reported by [33], where viscoelastic creep reduced the effective critical load over time. A similar trend is observed in Equation 15, where increasing the Prony coefficient  $g$  leads to higher strain energy accumulation during the creeping process, and hence needs higher flow speed and energy to initiate buckling.

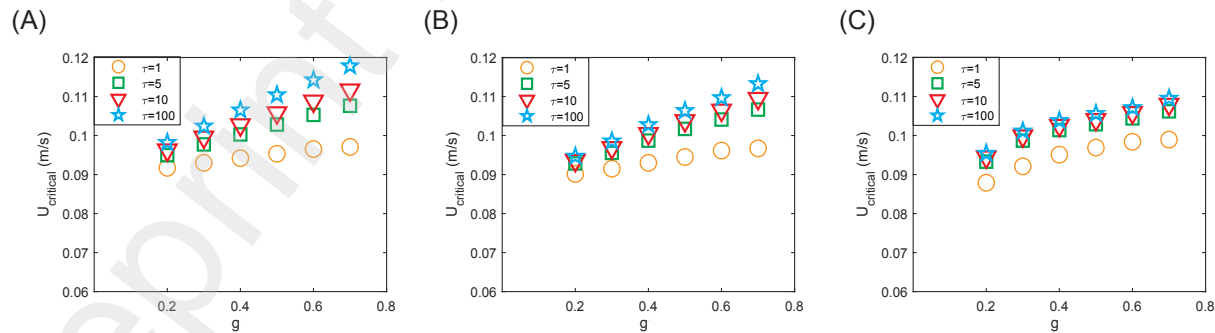


Figure 4: The variation of critical flow speed at maximum strain energy over Prony coefficient  $g$  at different inlet flow acceleration (A)  $q = 0.005$  m/s<sup>2</sup> (B)  $q = 0.01$  m/s<sup>2</sup> (C)  $q = 0.02$  m/s<sup>2</sup>

Meanwhile, as  $\tau$  increases to larger than around 10, Figure 4 (B)-(C) show the critical flow speed for buckling is hardly affected by the further increase of  $\tau$ . This is because at high

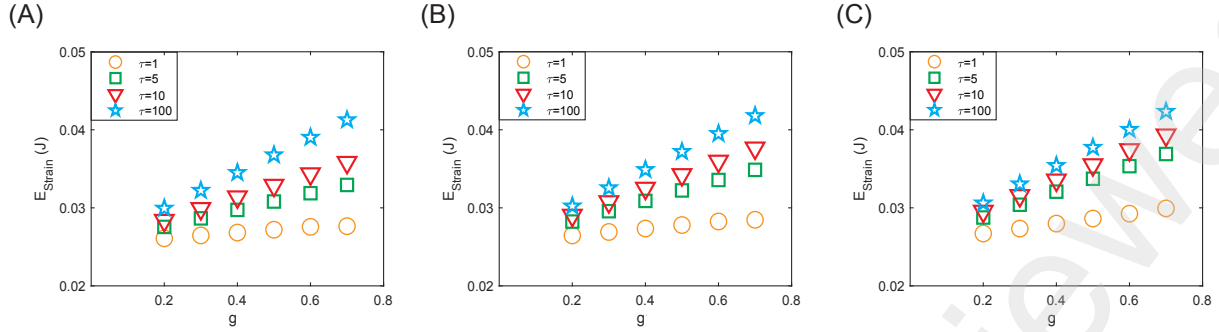


Figure 5: The variation of maximum strain energy over Prony coefficient  $g$  at different inlet flow acceleration (A)  $q = 0.005 \text{ m/s}^2$  (B)  $q = 0.01 \text{ m/s}^2$  (C)  $q = 0.02 \text{ m/s}^2$

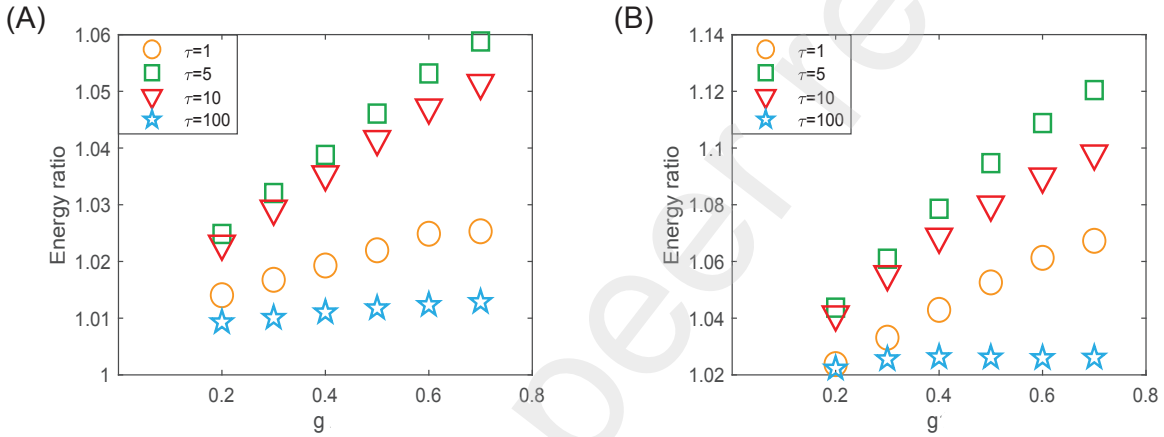


Figure 6: Ratio of maximum strain energy at increasing inlet flow accelerations relative to  $q = 0.005 \text{ m/s}^2$ , shown over Prony coefficient  $g$  for different relaxation times  $\tau$  (A)  $q = 0.01 \text{ m/s}^2$  (B)  $q = 0.02 \text{ m/s}^2$

inlet flow accelerations, the time to reach to the critical flow speed  $t_{\text{critical}}$  is decreased, and hence  $e^{-\frac{t_{\text{critical}}}{\tau}}$  approaches 1. Consequently, the structure approaches a fully elastic limit in which the effective Young's modulus is approximately  $2G_0(1 + \nu)$ . In these situations, the total maximum strain energy in the system still increases with the Prony coefficient  $g$ , as shown in Equation 15.

Figure 5 presents the maximum structural strain energy attained during the snap-through buckling process, with subfigures (A)–(C) corresponding to  $q = 0.005 \text{ m/s}^2$ ,  $0.01 \text{ m/s}^2$ , and  $0.02 \text{ m/s}^2$ , respectively. The variation in strain energy follows a similar trend to that of the critical flow speed shown in Figure 4. Specifically, the maximum strain energy increases with both the Prony coefficient  $g$  and the relaxation time  $\tau$ , indicating pronounced viscoelastic effects.

In the state close to fully elastic limit, corresponding to  $\tau = 100 \text{ s}$  and  $g = 0.7$  (blue stars), the strain energy reaches its highest values. Compared to the relaxed state ( $\tau = 1 \text{ s}$ , yellow circles), the maximum strain energy stored in the system can be up to approximately 1.6 times of the energy in relaxed state. This enhancement reflects the increased stiffness resulting from the dominance of elastic behavior in materials with long relaxation times and high  $g$  values.

Figure 6 shows the ratio of maximum strain energy at higher inlet flow accelerations compared to the baseline case of  $q = 0.005 \text{ m/s}^2$ . This ratio reflects how much additional energy the viscoelastic structure can store when the flow speed increases more quickly. As shown in Figure 6(B), the strain energy can increase by up to 12% when the  $q$  is increased 4 times of the baseline to  $q = 0.02 \text{ m/s}^2$ . This effect is most noticeable for intermediate values of relaxation time ( $\tau = 5\text{--}10 \text{ s}$ ) and higher  $g$ . When  $\tau = 1$  or  $\tau = 100$ , the strain energy changes very little with  $q$ , suggesting that materials with either very fast or very slow relaxation do not respond as much to changes in flow acceleration rates. These results show that viscoelastic materials can adjust how much energy they store depending on how quickly the flow changes, a behavior not observed in elastic materials, as shown in Figure 3.

### 6.3. The dimensionless parameters for the buckling of viscoelastic structure

The Cauchy number (Ca) is a key dimensionless parameter used to characterize fluid–structure interactions. It represents the ratio of fluid-induced inertial forces to the structural stiffness resisting deformation. For a linear elastic material, the Cauchy number is defined as

$$\text{Ca} = \frac{\rho U^2}{4E} \left( \frac{L}{d} \right)^3 \left( \frac{L}{h} \right),$$

where  $\rho$  is the fluid density,  $U$  is the characteristic flow velocity,  $E$  is the Young's modulus of the elastic material, and  $L$ ,  $d$ , and  $h$  are the beam's geometric parameters.

For viscoelastic bistable structures, the material stiffness varies with time due to relaxation effects. Therefore, the Cauchy number is reformulated using an effective modulus  $E_{\text{eff}}$ , yielding

$$\text{Ca} = \frac{\rho U^2}{4E_{\text{eff}}} \left( \frac{L}{d} \right)^3 \left( \frac{L}{h} \right), \quad (16)$$

where the effective modulus  $E_{\text{eff}}$  accounts for time-dependent viscoelastic behavior and is defined as

$$E_{\text{eff}} = 2(1 + \nu)G_0 \left[ 1 - g \left( 1 - e^{-\frac{t}{\tau}} \right) \right],$$

with  $G_0$  denoting the instantaneous shear modulus,  $\nu$  the Poisson's ratio,  $g$  the dimensionless Prony coefficient, and  $\tau$  the relaxation time. The time  $t$  is selected as the time to reach the local maximum of strain energy.

For the bistable beam undergoing snap-through buckling in fluid, the evolution of elastic strain energy was previously investigated in [7]. Accordingly, one of the key output metrics in this study is the dimensionless strain energy, defined as

$$E_{\text{strain}}^* = \frac{E_{\text{strain}}}{\frac{1}{2}E_{\text{eff}}I\kappa_0^2L}, \quad (17)$$

where  $\kappa_0 = 2h/L^2$  is the initial discrete curvature at the center of the beam, with  $h$  denoting the initial midpoint height. The parameter  $I$  is the second moment of area, which scales with  $d^3$ , and  $E_{\text{eff}}$  is the effective modulus of elasticity. In this paper, we choose the maximum strain energy to calculate  $E_{\text{strain}}^*$ .

Figure 7(A) presents the variation of the  $E_{\text{strain}}^*$  over the Ca. The data points are color-coded, with yellow, green, and red representing increasing  $q$  from  $0.005 \text{ m/s}^2$  to  $0.02 \text{ m/s}^2$ .

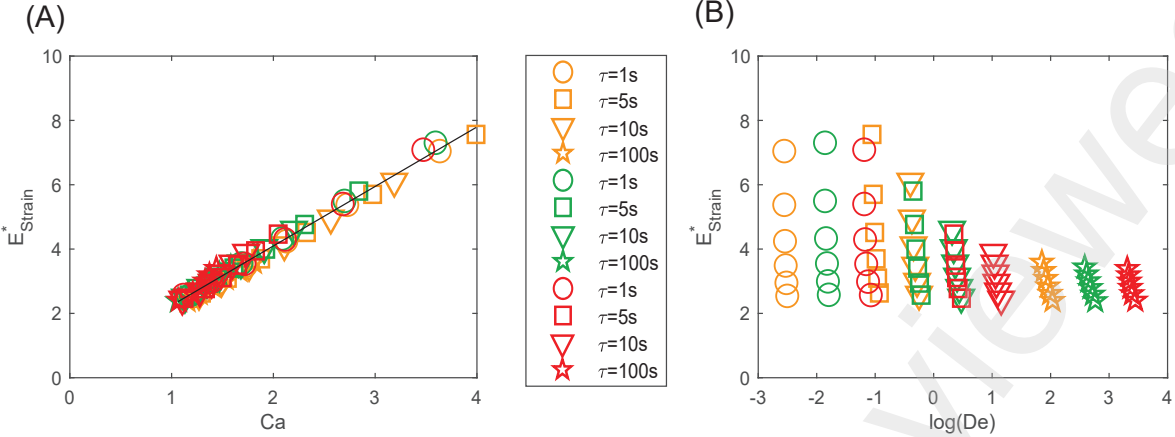


Figure 7: (A) The variation of  $E_{\text{strain}}^*$  over Ca with effective stiffness. A linear curve fitting is conducted on all the numerical simulated results (B) The variation of  $E_{\text{strain}}^*$  over  $\log(\text{De})$ .

The data exhibits a clear linear relationship between  $E_{\text{strain}}^*$  and Ca. A linear curve is found to fit the data perfectly, with an R-squared value reaching 0.98. The lowest Cauchy number required for initiating the viscoelastic structures' buckling is found to be near 1.

The Deborah number  $\frac{\tau}{t_{\text{obs}}}$  defined in Section 4 is also important for characterizing viscoelastic structures. Here, we used the time to reach the maximum strain energy as the  $t_{\text{obs}}$ . Figure 7(B) is a linear-log plot, where  $E_{\text{strain}}^*$  is plotted as a function of the logarithmic form of the Deborah number. The results indicate that for higher Deborah numbers, associated with more elastic behavior, the values of  $E_{\text{strain}}^*$  are tightly clustered, suggesting consistent elastic response. In contrast, for lower Deborah numbers, which represent more viscous behavior, the strain energy becomes more scattered and less predictable. This variability may be attributed to creep effects. At the lowest  $q$  with  $q = 0.005 \text{ m/s}^2$ , most data points fall in the  $\text{De} < 1$  regime, indicating viscous structural response. As the  $q$  increases, the structure transitions toward a more solid-like response, indicated by the shift to higher Deborah numbers.

In the following sections, we investigate the fluid-structure interaction process for the viscoelastic structures to understand its snap-through buckling in more detail.

#### 6.4. Analysis of structural dynamics and flow patterns at a slow inlet flow acceleration

We selected representative cases with  $q=0.005 \text{ m/s}^2$ ,  $g = 0.7$ , and  $\tau = 5$  second. As shown in Figure 6 (B), this case is found to be the case most sensitive to the variation in the inlet flow accelerations. In this flow condition, the corresponding Cauchy number is 4, and the Deborah number is 0.35. The material is viscous dominated. Figure 8 presents the variation of the structural displacement and strain energy at the center point of the beam. The structure experiences a fast buckling with the center point displaced by 50 mm within around 2 seconds. After this process, the structure will oscillate around the other energy minimum state until it remains stationary. The star symbols highlight the representative states (A)-(D), covering the four stages of the snap-through buckling process. Figure 9 presents the corresponding pressure field with streamlines in the representative states (A)-(D). The spatial distributions of the structural velocity are compared in Figure 10. In the initial stages, the fluid pressure

is distributed uniformly along the structure, as presented in Figure 9 (A). As the velocity at the center point increases in Figure 10(B-D), the local flow velocity also increases, and hence, the pressure near the center point continuously decreases, according to Bernoulli's principle. Counter-rotating vortices are formed in the wake of the structure. When the structure moves past the maximum strain energy state, the local velocities of the structure are out of phase with the local hydrodynamic load. This suggests that the total hydrodynamic power is negative. Even without positive external energy input, the structure can continue moving in the positive X direction because of the release of stored strain energy. We also studied flow features of different material properties at this inlet flow acceleration rate, and we didn't find significantly different flow features.

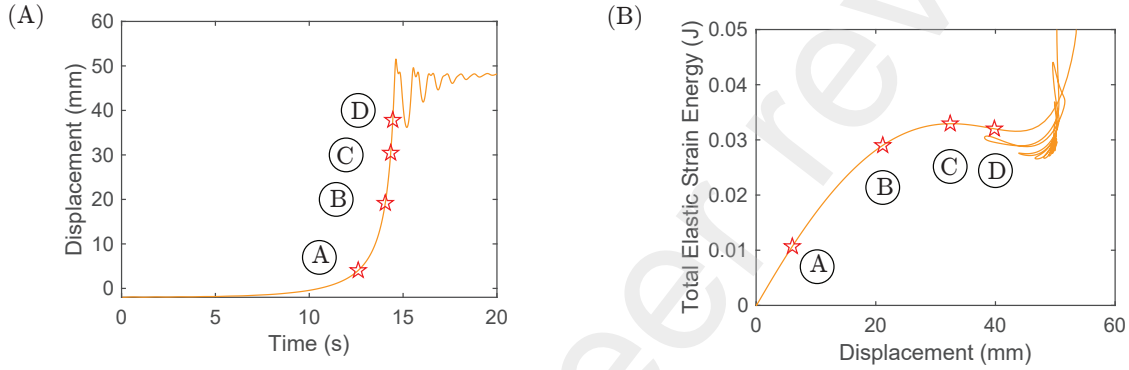


Figure 8: (A) The structural displacement at the center point versus time with  $q = 0.005 \text{ m/s}^2$  (B) The total elastic strain energy versus structural displacement at the center point. The corresponding structural representative states are denoted by star symbols.

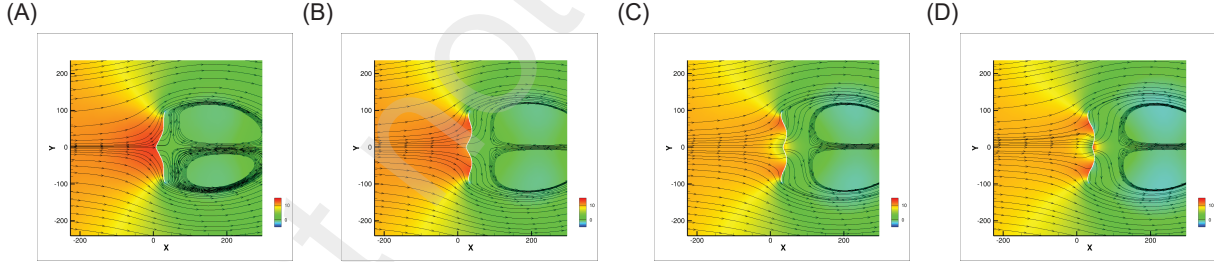


Figure 9: The corresponding pressure field at the representative structural positions. Columns (A-D) represent the flow conditions at representative states A-D in Figure 8

### 6.5. Analysis of structural dynamics and flow patterns at a fast inlet flow acceleration

To understand why a faster change in flow velocity enables the viscoelastic structure to store more strain energy, as shown in Figure 6, we study the same material from Section 6.4, now with a higher  $q$ , at  $q = 0.02 \text{ m/s}^2$ . Under this condition, the corresponding Cauchy number is 2.05, and the Deborah number is 1.41, which is more elastic. Figure 11 presents the variation of the structural displacement at the center and the total elastic strain energy. Compared to the case with a slower  $q$ , the flow-induced structure deformation initiates at

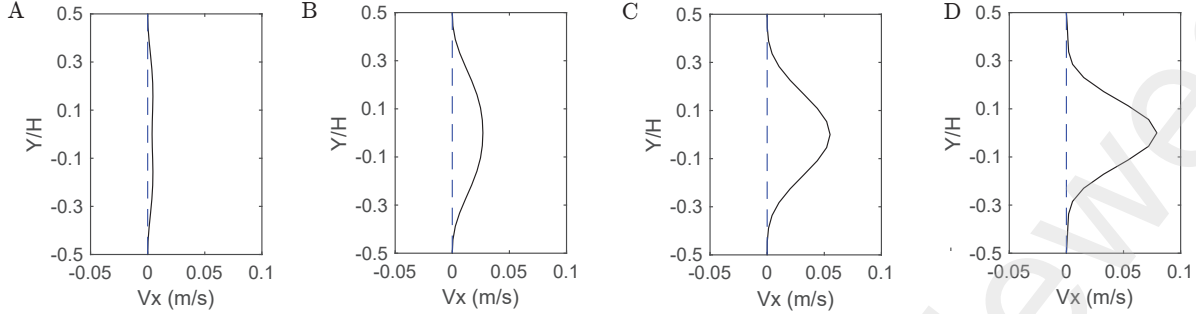


Figure 10: (A-D) Distributions of structural horizontal velocity along the vertical position of the beams at flow states A-D in Figure 8.

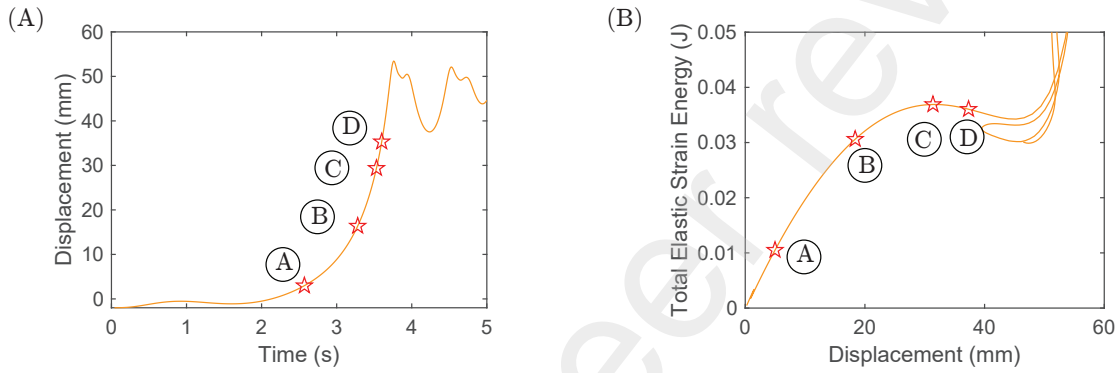


Figure 11: (A) The structural displacement at the center point versus time with  $q = 0.02 \text{ m/s}^2$  (B) The total elastic strain energy versus structural displacement at the center point. The corresponding structural representative states are denoted by star symbols.

a lower flow speed, and the structure stores more strain energy. Four representative states (A–D) are highlighted using star markers; these points are chosen to align with the same displacement level at point C in Figure 8, allowing direct comparison between slow and fast flow acceleration responses.

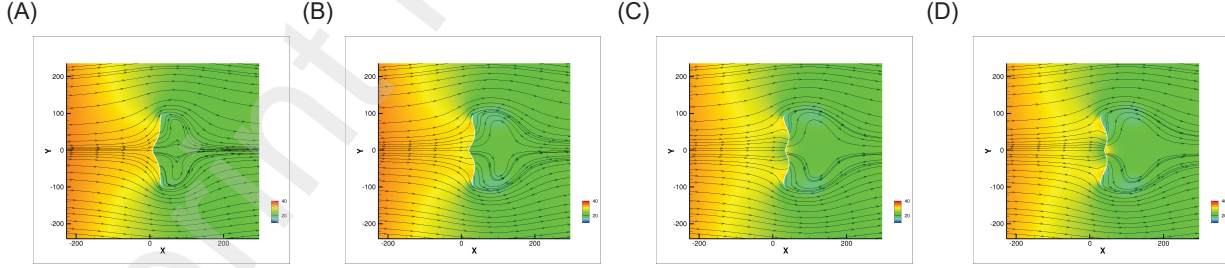


Figure 12: The corresponding pressure field at the representative structural positions. Columns (A-D) represent the flow conditions at representative states A-D in Figure 11

Figure 12 shows the pressure fields and streamlines corresponding to the highlighted structural states. Compared to the slower flow-rate case in Figure 9, the streamlines here exhibit tighter convergence near the structure and more pronounced curvature around the wake. Weak recirculation is observed in the wake, likely due to the high fluid acceleration.

The resulting strong adverse pressure gradient suppresses vortex development, preventing the recirculation zones from growing significantly.

The curved streamlines indicate an increased pressure gradient along the horizontal direction. Figure 13 shows the horizontal velocity distribution along the vertical cross-section of the beam at four representative states. Compared to Figure 10, the structure moves at a faster rate, causing the fluid to accelerate near its center. The combined effect of the stronger pressure gradient and increased structural velocity results in greater energy being transferred from the fluid flows to the structures.

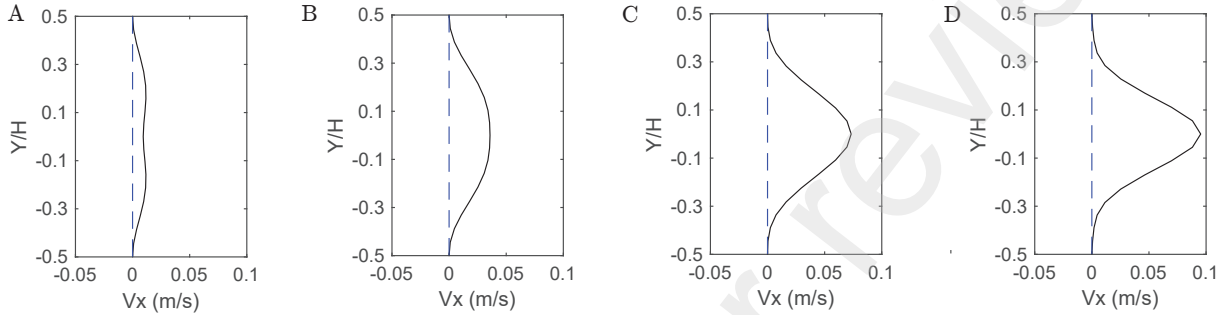


Figure 13: (A-D) Distributions of structural horizontal velocity along the vertical position of the beams at flow states A-D in Figure 11.

## 7. Conclusions

This paper studies the snap-through buckling phenomena of viscoelastic bistable beams in time varying fluid flows. We systematically studied the effect of the Prony coefficients and relaxation time constants on the snap-through buckling behavior under different rates of change of flow velocity. As the relaxation time increases, the material exhibits more elastic behavior and requires greater flow-induced energy to initiate buckling. Delayed buckling is observed with increasing Prony coefficient, indicating the influence of creep effects.

For conventional elastic structures, snap-through buckling dynamics and strain energy storage are largely unaffected by the flow acceleration rate. In contrast, for viscoelastic structures, increasing the flow acceleration rate leads to a more rapid rise in strain energy, making the structure behave as if it were stiffer. This behavior stems from a transition from a viscous-dominated to an elastic-dominated regime as the hydrodynamic loading rate increases. Detailed fluid-structure interaction analysis further reveals that at higher flow acceleration, the streamlines are more deflected, and the pressure gradient is increased along the flow direction, resulting in enhanced local loading and greater structural velocity during snap-through.

Two important dimensionless parameters were discussed. First, we found that the Cauchy number, modified by the effective viscoelastic stiffness, governs the dimensionless strain energy during buckling. The viscoelastic structure initiates snap-through buckling once the Cauchy number exceeds a critical threshold near 1. Second, the Deborah number characterizes the relative importance of elasticity versus viscosity. As the Deborah number decreases—indicating more viscous behavior—the dimensionless strain energy exhibits larger variability. The insights revealed in this study provide a deeper understanding of how time-dependent material behavior and flow conditions interact to govern interesting structural

dynamics. These results can inform the design of adaptive viscoelastic systems for applications in underwater vehicles, soft robotics, and morphing structures where environmental flow conditions vary dynamically.

## 8. Acknowledgements

L.M. acknowledges the support for her startup funding from Ira A. Fulton Schools of Engineering at Arizona State University, support from USDA Award No.2024-67021-42526, and Early Career Fellowship in Gulf Research Program from the National Academy of Sciences, Engineering, and Medicine.

## Appendix A. Validation of the viscoelastic materials

The viscoelastic material properties of VytaFlex 20 (V20) were obtained from stress relaxation experiments reported in [34]. The experimental data were approximated using a two-branch Prony series with an initial shear modulus of 172 kPa. The identified Prony coefficients are  $g_1 = 0.2039$  with a relaxation time  $\tau_1 = 4.4193$  s, and  $g_2 = 0.1632$  with  $\tau_2 = 100.1317$  s. For the present validation, a simplified one-branch Prony series was employed to model viscoelastic stress relaxation behavior during the tensile test simulation.

To validate the theoretical model, a finite element analysis (FEA) was performed in COMSOL Multiphysics to simulate the uniaxial tensile stress relaxation of VytaFlex 20. A time-dependent tensile strain of 20% was applied over 1 second and held constant for an additional 30 seconds. The corresponding stress response was recorded and compared with the theoretical prediction obtained by convolving the strain history with the relaxation modulus  $E(t)$ , defined as:

$$E(t) = E_0 \left( 1 - \sum_{i=1}^n g_i (1 - e^{-t/\tau_i}) \right), \quad (\text{A.1})$$

where  $E_0$  is the instantaneous Young's modulus of VytaFlex 20, computed based on Equation 10.

Figure Appendix A.1 presents the validation results. The left panel shows the FEA simulation setup, while the right panel compares the stress relaxation curves obtained from the theoretical model and the FEA simulation. The close agreement between the two confirms the accuracy of the viscoelastic model in capturing the time-dependent mechanical response of VytaFlex 20.

## References

- [1] Y. Chen, T. Liu, L. Jin, Spatiotemporally programmable surfaces via viscoelastic shell snapping, *Advanced Intelligent Systems* 4 (2022) 2100270. doi:10.1002/aisy.202100270.
- [2] M. Munegkar, L. Ma, W. Yan, V. Kackar, S. Shokrazadeh, M. K. Jawed, Design of bistable soft deployable structures via a kirigami-inspired planar fabrication approach, arXiv preprint arXiv:2301.09179 (2023).

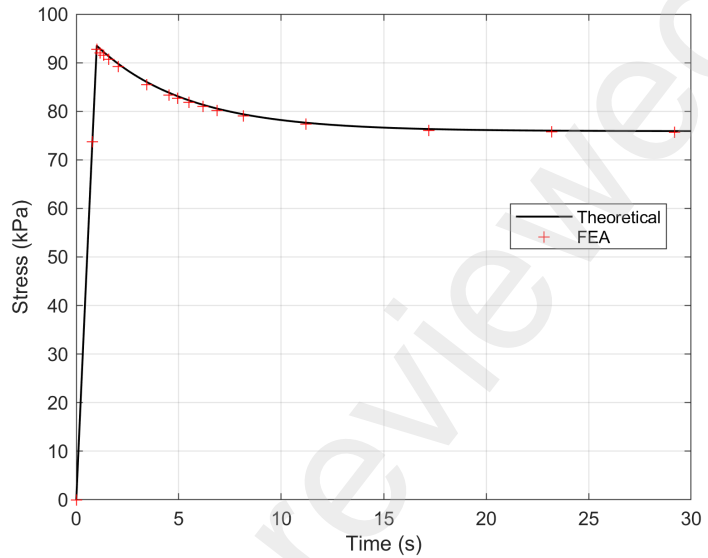
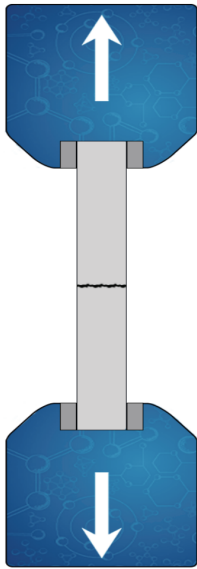


Figure Appendix A.1: Validation of the viscoelastic material. Left: Setup for the numerical experiment. Right: Stress relaxation response under tensile testing.

- [3] Y. Chi, Y. Li, Y. Zhao, Y. Hong, Y. Tang, J. Yin, Bistable and multistable actuators for soft robots: Structures, materials, and functionalities, *Advanced Materials* 34 (19) (2022) 2110384.
- [4] D. K. Patel, X. Huang, Y. Luo, M. Mungekar, M. K. Jawed, L. Yao, C. Majidi, Highly dynamic bistable soft actuator for reconfigurable multimodal soft robots, *Advanced Materials Technologies* 8 (2) (2023) 2201259.
- [5] S. Coyle, C. Majidi, P. LeDuca, K. J. Hsia, Bio-inspired soft robotics: Material selection, actuation, and design, *Extreme Mechanics Letters* 22 (2018) 51–59. doi:10.1016/j.eml.2018.05.004.  
URL <https://www.sciencedirect.com/science/article/pii/S2352431617302316>
- [6] M. Gomez, D. Moulton, D. Vella, Dynamics of viscoelastic snap-through (07 2018).
- [7] L. Ma, W. Chen, R. Zha, A. H. Escobar, Flow-induced buckling of a bistable beam in uniform flow, *Journal of Fluids and Structures* 131 (2024) 104220.
- [8] H. Kim, M. Lahooti, J. Kim, D. Kim, Flow-induced periodic snap-through dynamics, *Journal of Fluid Mechanics* 913 (2021) A52.
- [9] Q. Mao, Y. Liu, H. J. Sung, Snap-through dynamics of a buckled flexible filament in a uniform flow, *Journal of Fluid Mechanics* 969 (2023) A33.
- [10] Z. Chen, Q. Mao, Y. Liu, H. J. Sung, Snap-through dynamics of a buckled flexible filament in a channel flow, *Physics of Fluids* 36 (1) (2024).
- [11] T. Resvanis, Vortex-induced vibration of flexible cylinders in time-varying flows, Ph.D. thesis (09 2014).

- [12] J. K. Vandiver, L. Ma, Does more tension reduce viv?, in: International Conference on Offshore Mechanics and Arctic Engineering, Vol. 57700, American Society of Mechanical Engineers, 2017, p. V05BT04A039.
- [13] J. K. Vandiver, L. Ma, Z. Rao, Revealing the effects of damping on the flow-induced vibration of flexible cylinders, *Journal of Sound and Vibration* 433 (2018) 29–54.
- [14] Y. Chen, T. Liu, L. Jin, Pseudo-bistability of viscoelastic shells., *Philosophical transactions. Series A, Mathematical, physical, and engineering sciences* 381 (2023) 20220026.
- [15] M. Gomez, D. E. Moulton, D. Vella, Dynamics of viscoelastic snap-through, *Journal of the Mechanics and Physics of Solids* 124 (2019) 781–813.
- [16] M. A. Kraus, M. Schuster, J. Kuntsche, G. Siebert, J. Schneider, Parameter identification methods for visco- and hyperelastic material models, *Glass Structures Engineering* 2 (2) (2017) 147–167. doi:10.1007/s40940-017-0042-9.  
URL <https://doi.org/10.1007/s40940-017-0042-9>
- [17] Q. Zhong, J. Zhu, F. E. Fish, S. J. Kerr, A. Downs, H. Bart-Smith, D. Quinn, Tunable stiffness enables fast and efficient swimming in fish-like robots, *Science Robotics* 6 (57) (2021) eabe4088.
- [18] L. Song, S. Fu, Y. Zeng, Y. Chen, Hydrodynamic forces and coefficients on flexible risers undergoing vortex-induced vibrations in uniform flow, *Journal of Waterway, Port, Coastal, and Ocean Engineering* 142 (4) (2016) 04016001.
- [19] L. Song, S. Fu, J. Cao, L. Ma, J. Wu, An investigation into the hydrodynamics of a flexible riser undergoing vortex-induced vibration, *Journal of Fluids and Structures* 63 (2016) 325–350.
- [20] B. Yang, R. Baines, D. Shah, S. Patiballa, E. Thomas, M. Venkadesan, R. Kramer-Bottiglio, Reprogrammable soft actuation and shape-shifting via tensile jamming, *Science Advances* 7 (40) (2021) eabh2073. doi:10.1126/sciadv.abh2073.  
URL <https://www.science.org/doi/10.1126/sciadv.abh2073>
- [21] R. E. Corman, L. Rao, N. Ashwin Bharadwaj, J. T. Allison, R. H. Ewoldt, Setting material function design targets for linear viscoelastic materials and structures, *Journal of Mechanical Design* 138 (5) (2016) 051402. arXiv:[https://asmedigitalcollection.asme.org/mechanicaldesign/article-pdf/138/5/051402/6227889/md\\_138\\_05\\_051402.pdf](https://asmedigitalcollection.asme.org/mechanicaldesign/article-pdf/138/5/051402/6227889/md_138_05_051402.pdf), doi:10.1115/1.4032698.  
URL <https://doi.org/10.1115/1.4032698>
- [22] L. Ma, M. Munegkar, V. Roychowdhury, M. K. Jawed, Rapid design of fully soft deployable structures via kirigami cuts and active learning, *arXiv preprint arXiv:2303.11295* (2023).
- [23] C. Multiphysics, Introduction to comsol multiphysics®, COMSOL Multiphysics, Burlington, MA, accessed Feb 9 (2018) (1998) 32.

- [24] O. H. Yeoh, Some forms of the strain energy function for rubber, *Rubber Chemistry and technology* 66 (5) (1993) 754–771.
- [25] C. Renaud, J.-M. Cros, Z.-Q. Feng, B. Yang, The Yeoh model applied to the modeling of large deformation contact/impact problems, *International Journal of Impact Engineering* 36 (5) (2009) 659–666.
- [26] Y. A. Mayi, A. Queva, M. Dal, G. Guillemot, C. Metton, C. Moriconi, P. Peyre, M. Bellet, Multiphysics simulation of single pulse laser powder bed fusion: comparison of front capturing and front tracking methods, *International Journal of Numerical Methods for Heat & Fluid Flow* 32 (6) (2022) 2149–2176.
- [27] A. Goza, T. Colonius, J. E. Sader, Global modes and nonlinear analysis of inverted-flag flapping, *Journal of Fluid Mechanics* 857 (2018) 312–344.
- [28] M. Reiner, The deborah number, *Physics today* 17 (1) (1964) 62–62.
- [29] E. Lauga, Life at high deborah number, *Europhysics Letters* 86 (6) (2009) 64001.
- [30] S. Turek, J. Hron, Proposal for numerical benchmarking of fluid-structure interaction between an elastic object and laminar incompressible flow, Springer, 2006.
- [31] F. Gosselin, E. De Langre, B. A. Machado-Almeida, Drag reduction of flexible plates by reconfiguration, *Journal of Fluid Mechanics* 650 (2010) 319–341.
- [32] T. L. Resvanis, Vortex-induced vibration of flexible cylinders in time-varying flows, Ph.D. thesis, Massachusetts Institute of Technology (2014).
- [33] L. Stein-Montalvo, D. P. Holmes, G. Coupier, Delayed buckling of spherical shells due to viscoelastic knockdown of the critical load, *Proceedings of the Royal Society A* 477 (2253) (2021) 20210253.
- [34] Y. Chen, T. Liu, L. Jin, Spatiotemporally programmable surfaces via viscoelastic shell snapping, *Advanced Intelligent Systems* (2022) 2100270.